Electronic polarization effects on charge carriers in anthracene: A valence bond study

Frédéric Castet,[1,*,†] Philippe Aurel,[1] Alain Fritsch,[1] Laurent Ducasse,[1] Daniel Liotard,[1] Mathieu Linares,[1,2] Jérôme Cornil,[2] and David Beljonne[1,2,*,‡]

[1]*Institut des Sciences Moléculaires, UMR CNRS 5255, Université Bordeaux I, 351 Cours de la Libération, F-33405 Talence, France*

[2]*Laboratory for Chemistry of Novel Materials, University of Mons-Hainaut, Place du Parc 20, B-7000 Mons, Belgium*

(Received 11 July 2007; revised manuscript received 25 January 2008; published 24 March 2008)

A semiempirical quantum-chemical model based on a fragment orbital formalism is presented to assess molecular parameters relevant to charge transport in organic crystals. The mixed valence bond/Hartree–Fock approach provides an efficient integrated framework to evaluate the electronic polarization effects induced by localized charge carriers and the associated impact on the matrix elements mediating electron migration in the hopping regime. This formalism, applied here to anthracene clusters of increasing sizes and dimensionalities, yields the electrostatic and polarization contributions to the total interaction energy of the neutral and charged aggregates and leads to a reduction in the effective bandwidth by $\sim 10\% - 20\%$ as a result of the polarization cloud.

DOI: 10.1103/PhysRevB.77.115210 PACS number(s): 72.80.Le

I. INTRODUCTION

The design and development of optoelectronic devices based on organic conjugated molecules and polymers have led to the emergence of the field of organic electronics. The envisioned applications comprise, among others, electroluminescent diodes for displays and lighting, field-effect transistors for logic circuits, photovoltaic cells for energy conversion, and sensors for the detection of (bio)chemical species. It is the combination of the unique electronic and optical properties of conjugated systems with the typical characteristics of organic materials (tailored synthesis, easy processing, low cost, etc.) that makes conjugated materials so attractive for such applications.[1]

Although some devices are already on the market place, a detailed understanding of key electronic processes involved in their working principle is still lacking. This is the case for the mechanism of charge transport in organic crystals at room temperature, which is the focus of the present contribution. In that respect, molecular modeling is a useful tool that is expected to provide a deep insight into the relationship between the chemical structure of the organic molecules and polymers and their optoelectronic properties. Charge transport has been largely studied at a fundamental level in molecular crystals due to their well-defined structure. It has been shown to operate in a band regime similar to that in inorganic semiconductors only at low temperatures and in the absence of impurities.[2] An increase in the temperature leads to a progressive localization of the charge carriers that is triggered by the thermal activation of the lattice phonons; the coherent motion is then lost in the presence of fluctuations both in the site energies of the carriers (dynamic diagonal disorder) and in the amplitude of the transfer integrals (dynamic nondiagonal disorder) that electronically couple adjacent molecules.[3–5] Ultimately, the charge carriers get localized over a single molecule and migrate across the molecular crystal through a sequence of successive hopping events. The hopping regime is further reinforced by the presence of *static* diagonal and nondiagonal disorders. We focus here on such a localized picture, which appears as a good starting point to describe charge transport in most organic crystals at room temperature.

At the semiclassical limit, the rate of charge hopping between two interacting molecules is given in the framework of the Marcus theory as[6]

$$k_{if} = \frac{2\pi}{\hbar} t^2 \frac{1}{\sqrt{4\pi\lambda k_B T}} \exp[-(\Delta G^0 + \lambda)^2/4\lambda k_B T]$$

with t the transfer integral, λ the total reorganization energy, and ΔG^0 the free enthalpy of the reaction that results from the application of an external electric field[7] and/or the presence of static energy disorder; this latter contribution implies that the energy of the charge is different on the initial and final sites and requires the total electronic energy of a charged molecule within the crystal to be calculated, with an explicit account of electrostatic and polarization effects. Note that (i) electronic polarization effects are generally assumed to be instantaneous in electron transfer theories and, hence, should not contribute to the energy barrier introduced by the reorganization energy (which is governed by intramolecular geometric relaxation effects for the internal part and changes in the nuclear polarization of the neighboring molecules for the external part); (ii) statement (i) is only strictly valid in a frozen lattice environment, while in the dynamic case the fluctuations in electronic reorganization induced by nuclear motion might also contribute to the total reorganization energy.

The underlying difficulties in describing transfer integrals and the amplitude of a static energetic disorder are related to the overwhelming size of a the electronic cloud of the supramolecular system. To describe charge or excitation hopping over various molecular fragments, it is therefore desirable to develop quantum-chemical approaches that achieve a consistent partitioning of the electronic cloud to allow for the introduction of a chemically relevant effective Hamiltonian whose parameters describe local interactions between the molecular units.[8]

Recently, we have developed a semiempirical quantum-chemical model to consistently evaluate the electronic pa-

rameters relevant for charge transport in supramolecular systems, such as molecular crystals or biological macromolecules. In this model, the system is treated as a collection of weakly interacting molecular fragments. The formalism is based on the locality constraint of the fragment orbitals, allowing for a particular assignment of the electrons over the various atom groups. Different charge configurations can be identified as charge-transfer states of the system, in the spirit of a multiconfigurational valence bond (VB) approach. The underlying scheme relies on the group function formalism, in which the electronic states of the system result from the superposition of the fragment states. In the simplest description, the fragment ground state is treated at the Hartree–Fock (HF) level. This mixed VB/HF model was applied to study the charge-transfer properties of organic superconductors based on Bechgaard salts[9–11] and, more recently, hole delocalization within double-stranded DNA.[12–14]

The VB/HF scheme is applied here to evaluate the electrostatic interaction energies between molecular fragments as well as the amplitude of electronic polarization effects induced by localized charge carriers in the surrounding molecules in anthracene crystalline clusters of different shapes and sizes. In addition, the impact of the electronic polarization cloud on the hopping matrix elements between neighbor molecules has been assessed.

II. VALENCE BOND/HARTREE–FOCK MODEL

A. Basic equations

The VB/HF method was described in detail in a recent review.[15] We present here the general lines of the theoretical procedure to allow the reader a more complete comprehension of the results reported in the following sections. The wave functions describing the stationary electronic states of a supramolecular stack involving N weakly interacting fragments are expressed in an active configurational space built from single determinantal many-electron wave functions Φ_κ associated with the distinct charge-transfer states of the system,

$$\Psi = \sum_\kappa C_\kappa \Phi_\kappa. \tag{1}$$

These charge-transfer states, also referred to as VB configurations, correspond to a particular assignment of the electrons over the various fragments, each fragment R containing n_R electrons. When considering small overlaps between the electronic clouds of the various fragments, the spin orbitals can be chosen to be strictly localized on a single subsystem. This is practically achieved by requiring each orbital involved in the VB configurations to be expanded on the atomic orbitals of one and only one fragment R. We use here either the MINDO/3 (Ref. 16) method, based on the molecular intermediate neglect of differential overlap approximation, or MNDO (Ref. 17), AM1 (Ref. 18) and PM3 (Ref. 19) methods, all based on the neglect of diatomic differential overlap (NDDO) approximation. Accordingly, the set of spin orbitals of the N-group system can be strictly partitioned into N disjoint and nonoverlapping subsets that are described by their own wave function. When considering each group in its ground state, the N-group function Φ_κ can be expressed as a single generalized product of group functions ϕ_κ^R built from their own spin orbitals,

$$\Phi_\kappa = MA(\phi_\kappa^A \phi_\kappa^B, \ldots, \phi_\kappa^N), \tag{2}$$

where M is a normalizing factor and A ensures the antisymmetry of the functions Φ_κ with respect to the permutation of electrons belonging to different groups (the group functions ϕ_κ^R are assumed to be individually antisymmetric). As a result of the local and orthonormality character of the spin orbitals of the different groups, the N-group functions Φ_κ are orthonormalized. The VB matrix elements are thus given by

$$H_{\kappa\eta} = \langle \Phi_\kappa | \hat{H} | \Phi_\eta \rangle, \tag{3}$$

where the Hamiltonian operator describes the N-group system.

Within a VB/HF calculation, each group function associated with a given fragment implies only one determinant corresponding to the occupation of the lowest-energy spin orbitals. The spatial orbitals φ_i^R of each subsystem R are then optimized depending both on the net charge of the fragment and on the electrostatic field of all neighboring groups, following a local self-consistent field (SCF) optimization procedure. The diagonal terms $H_{\kappa\kappa}$ are the electronic energies associated with the various VB configurations. In the adopted semiempirical approximations, the exchange interactions between groups are not explicitly included, so that the diagonal terms $H_{\kappa\kappa}$ reduce to the sum of isolated fragment energies and of electrostatic interactions between electron densities of group pairs,

$$H_{\kappa\kappa} = \sum_R \langle \phi_\kappa^R | \hat{H}_R | \phi_\kappa^R \rangle + \frac{1}{2} \sum_R \sum_{S \neq R} \langle \phi_\kappa^R | \hat{J}^S | \phi_\kappa^R \rangle, \tag{4}$$

where the Hamiltonian operator $\hat{H}^R$ describes group R alone and the Coulomb operator $\hat{J}^S$ is related to group S.

We consider in this work the migration of a single electron or of a single hole within a hopping picture. The net charge of each fragment R can then be either 0, +1, or −1, so that the charged fragment is described by two electronic shells: The closed shell collecting all the doubly occupied molecular orbitals (MOs) and the open shell containing a single MO, which is assumed to be the highest occupied. The electronic structure of the charged groups is described within the framework of the restricted open shell Hartree–Fock formalism.[20] Two stationary conditions are involved in the self-consistent optimization procedure due to the treatment of two coupled Fock equations for the closed and open shells, respectively. The orthogonality constraints between MOs of the two shells are ensured by using a projection scheme of the open shell orbitals onto the subspace spanned by the virtual orbitals obtained from the closed shell equation.[9]

The coupling matrix elements that are relevant for charge transport are given by the off-diagonal terms $H_{\kappa\eta}$ between distinct VB configurations κ and η [Eq. (3)], which differ by the displacement of one charge from a molecular fragment to

a neighboring one. The calculation of these terms requires the evaluation of the overlap matrix $\mathbf{S}^{\kappa\eta}$ between the occupied spin orbitals involved in the two configurations κ and η. Indeed, these two sets of MOs being obtained from independent SCF processes, they are *a priori* nonorthogonal. Within the MINDO or NDDO schemes, only the one-electron part gives a nonzero contribution that can be written following Löwdin's extension to Slater rules for nonorthogonal MOs as[21]

$$H_{\kappa\eta} = \sum_{R,S} \sum_{i,j} (-1)^{i+j} \det(S_{i,j}^{\kappa\eta}) \cdot \langle \varphi_{\kappa,i}^{R} | \hat{h} | \varphi_{\eta,j}^{S} \rangle, \tag{5}$$

where $\hat{h}$ is the one-electron operator of the supramolecular system, and $\det(S_{i,j}^{\kappa\eta})$ the cofactor of the overlap matrix $\mathbf{S}^{\kappa\eta}$, say, the determinant of the matrix obtained after removing the line and column corresponding to the MOs $\varphi_{\kappa,i}^{B}$ and $\varphi_{\eta,j}^{A}$, respectively. Note that the $H_{\kappa\eta}$ terms measure the coupling between two many-electron wave functions and should be distinguished from the monoelectronic transfer integrals, $\langle \varphi_{\kappa,i}^{R} | \hat{h} | \varphi_{\eta,j}^{S} \rangle$, between individual MOs of the two fragments R and S. Due to the local and disjoint nature of the MOs, the overlap matrices are block diagonal in the MO basis (each block corresponding to a specific electron group describing a molecular fragment), and nonzero contributions in Eq. (5) arise only when fragments R and S correspond to the two units involved in the charge-transfer process, respectively. Moreover, as detailed in our previous works,[10,12] the VB/HF coupling matrix elements are proportional to the sum of the overlap contributions of the interacting fragments orbitals, with the major contribution arising from the two highest occupied molecular orbitals (HOMOs) (lowest unoccupied molecular orbitals) in the case of hole (electron) transport.

B. Partitioning of the interaction energy

Equation (4) shows that the total interaction energy between molecular fragments in an N-group cluster within the VB/HF method can be expressed as a sum of interactions between electron densities of fragment pairs. In turn, this electrostatic interaction energy can be partitioned into two distinct contributions; the first corresponds to interactions between the frozen electron densities of each pair of fragments, i.e., without any rearrangement of their electronic clouds, and the second to polarization effects due to the environment-induced orbital relaxation. These two contributions, hereafter denoted as E_{el} and E_{pol}, are referred to as electrostatic and dynamic polarization energies, respectively.

The $E_{\mathrm{el}}(N)$, $E_{\mathrm{el}}^{+}(N)$, and $E_{\mathrm{el}}^{-}(N)$ terms represent the electrostatic contribution to the total interaction energy in a neutral, positively, and negatively charged N-group systems, respectively. The difference $S^{+}(N)=E_{\mathrm{el}}^{+}(N)-E_{\mathrm{el}}(N)$ $[S^{-}(N)=E_{\mathrm{el}}^{-}(N)-E_{\mathrm{el}}(N)]$ can thus be interpreted as the difference in ionization energy (electron affinity) between the isolated fragment and the same fragment in electrostatic interactions with a molecular environment (excluding any effect provided by electronic cloud reorganization). Practically, the E_{el} terms are calculated as follows:

$$E_{\mathrm{el}}(N) = H_{\kappa\kappa}^{\mathrm{frozen}} - \sum_{R=1}^{N} \langle \phi_{\kappa}^{R_{\mathrm{isol}}} | \hat{H}^{R_{\mathrm{isol}}} | \phi_{\kappa}^{R_{\mathrm{isol}}} \rangle. \tag{6}$$

The first term $H_{\kappa\kappa}^{\mathrm{frozen}}$ represents the total energy of the N-group system given by Eq. (4), in which the group functions $\phi_{\kappa}^{R_{\mathrm{isol}}}$ involve the orbitals of isolated fragments. The second term is the sum of the total energies of the isolated fragments, and $\hat{H}^{R_{\mathrm{isol}}}$ the corresponding Hamiltonian operator. Since the group functions involved in the two terms are identical, Eq. (6) can be simplified into

$$E_{\mathrm{el}}(N) = \frac{1}{2} \sum_{R=1}^{N} \left\langle \phi_{\kappa}^{R_{\mathrm{isol}}} \left| \sum_{S \neq R}^{N} \hat{J}^{S_{\mathrm{isol}}} \right| \phi_{\kappa}^{R_{\mathrm{isol}}} \right\rangle. \tag{7}$$

The $E_{\mathrm{pol}}(N)$, $E_{\mathrm{pol}}^{+}(N)$, and $E_{\mathrm{pol}}^{-}(N)$ terms represent the dynamic electronic polarization contribution to the total interaction energy in a neutral, positively, and negatively charged N-group system, respectively. The difference $D^{+}(N)=E_{\mathrm{pol}}^{+}(N)-E_{\mathrm{pol}}(N)$ $[D^{-}(N)=E_{\mathrm{pol}}^{-}(N)-E_{\mathrm{pol}}(N)]$ yields the change in the ionization energy (electron affinity) of a given fragment, as induced by orbital relaxation due to the presence of a positive (negative) charge surrounded by polarizable molecules. The E_{pol} terms are calculated by taking the difference between the cluster total energies estimated from frozen and relaxed fragment orbitals, respectively,

$$E_{\mathrm{pol}}(N) = H_{\kappa\kappa} - H_{\kappa\kappa}^{\mathrm{frozen}}. \tag{8}$$

III. ELECTROSTATIC AND POLARIZATION ENERGIES IN ANTHRACENE CLUSTERS

Anthracene clusters have been built from the x-ray single crystal structure at $T=94$ K.[22] The unit cell, with parameters $a=8.4144$ Å, $b=5.9903$ Å, $c=11.0953$ Å, and $\beta=125.293°$, contains two independent molecules. One-dimensional (1D) clusters have been built along the b and $a+b$ crystal axes in which the molecules present a parallel and a herringbone (HB) stacking, respectively (see Fig. 1). Two-dimensional (2D) clusters of radius R have been built in the (a,b) plane and centered on the positively or negatively charged molecule. A given fragment is included into the cluster if the distance between one of its atoms and the center of mass of the central fragment is smaller than R. Similarly, increasingly large three-dimensional (3D) clusters of spherical shapes are built as onion skins.

A. Electrostatic interactions

Calculations were first performed on increasingly large monodimensional clusters containing an odd number of molecules, in which the positive or negative charge is confined on the central fragment (see Fig. 2). To address the influence of the semiempirical parametrization on the electrostatic interactions, calculations were carried out using either the MINDO/3 Hamiltonian or the three NDDO-type Hamiltonians, MNDO, AM1, and PM3. Hereafter, we only report the results obtained using the AM1 and MINDO/3 methods, as they are representative of the two different semiempirical formalisms used in this study. The complete set of data is

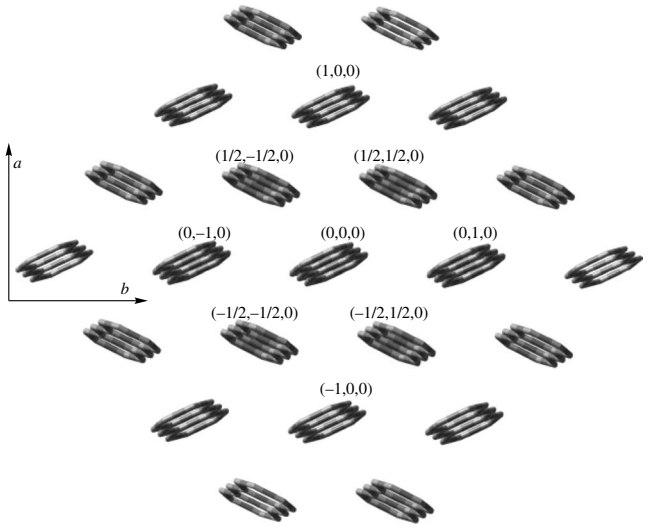

FIG. 1. View of a 2D anthracene cluster along the normal to the (a,b) plane and labeling of the nearest neighbors with respect to the central molecule.

available as supplementary information (Figs. S1–S5).[23]

Whatever the parametrization and the cluster shape (HB or parallel) are, the electrostatic energy per molecule, E_{el}/N, increases with N and converges toward a finite limit independent of the charge of the cluster [Fig. S1(a)]. However, asymptotic values strongly depend on the semiempirical parametrization [Fig. S1(b)]. In particular, it is noticeable that the molecular electrostatic contributions are much higher at the MINDO/3 level (E_{el}/N=415 meV in the infinite chain limit for a parallel stacking) compared to the other three parametrizations (E_{el}/N=48 meV at the AM1 level). For HB clusters, in which the intermolecular distance is smaller, the extrapolation to the infinite chain yields 806 and 145 meV within the MINDO/3 and AM1 levels, respectively. The difference in the asymptotic values, in fact, reflects the very different charge distributions provided by the two parametrizations (see Table I).

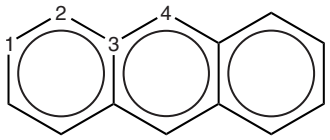

FIG. 2. Chemical structure of the anthracene molecule.

The differences between electrostatic interactions in a charged and a neutral cluster, i.e., $S^+=E_{el}^+-E_{el}$ and $S^-=E_{el}^-$ $-E_{el}$, are reported as a function of N in Fig. 3. Whatever the parametrization, S^+ and S^- cancel each other to within 10^{-3} eV. This is not surprising considering the Mulliken charge distributions in the neutral and charged molecules (Table I). Indeed, the changes in the atomic charges between the neutral and cationic forms are almost exactly opposite to those calculated between the neutral and anionic forms. Thus, as a consequence of the electron-hole symmetry, adding or removing an electron to a molecular fragment (while freezing the molecular orbitals) induces changes in the electrostatic potential that almost exactly compensate each other (within the numerical accuracy of the methods used).

Moreover, S^+ quickly saturates with the number of fragments. For both parallel and HB clusters, the PM3 param-

TABLE I. Mulliken charge distributions (in $|e|$) for neutral and charged anthracene molecules calculated using different semiempirical parametrizations. The atom numbering is shown in Fig. 2. Only one-fourth of the molecule is reported due to the D_{2h} symmetry. Atomic charges over united atoms (sum over C and H atoms) are given between parentheses.

	AM1				
	Neutral (N)	Cation (C)	Anion (A)	Difference, $N\rightarrow C$	Difference, $N\rightarrow A$
C1 (C1+H)	−0.127 (0.005)	−0.084 (0.091)	−0.168 (−0.079)	0.042 (0.085)	−0.041 (−0.085)
C2 (C2+H)	−0.118 (0.014)	−0.040 (0.127)	−0.198 (−0.100)	0.077 (0.112)	−0.081 (−0.115)
C3	−0.034	−0.080	0.018	−0.047	0.052
C4 (C4+H)	−0.107 (0.027)	0.058 (0.227)	−0.277 (−0.177)	0.165 (0.200)	−0.170 (−0.204)
H(C1)	0.132	0.175	0.089	0.043	−0.044
H(C2)	0.132	0.167	0.098	0.035	−0.034
H(C4)	0.134	0.169	0.100	0.035	−0.034
	MINDO/3				
	Neutral (N)	Cation (C)	Anion (A)	Difference, $N\rightarrow C$	Difference, $N\rightarrow A$
C1 (C1+H)	0.009 (0.003)	0.043 (0.087)	−0.024 (−0.081)	0.034 (0.084)	−0.032 (−0.083)
C2 (C2+H)	−0.003 (−0.012)	0.074 (0.100)	−0.083 (−0.127)	0.077 (0.112)	−0.080 (−0.115)
C3	0.022	−0.016	0.068	−0.038	0.046
C4 (C4+H)	−0.011 (−0.025)	0.146 (0.160)	−0.186 (−0.223)	0.157 (0.184)	−0.174 (−0.197)
H(C1)	−0.006	0.044	−0.057	0.050	−0.051
H(C2)	−0.009	0.026	−0.044	0.035	−0.035
H(C4)	−0.014	0.014	−0.037	0.027	−0.023

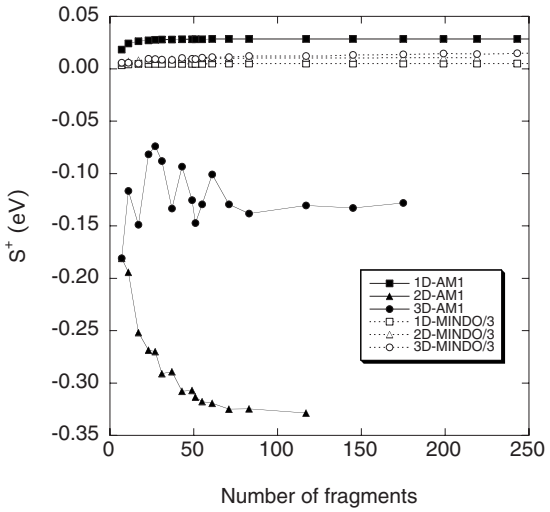

FIG. 3. Evolution of $S^+=E_{el}^+-E_{el}=-(E_{el}^--E_{el})$ as a function of the number of fragments for 1D (parallel), 2D and 3D clusters.

etrization gives rise to the highest absolute values of S^+ in the infinite chain limit (0.05 meV). The asymptotic values derived from VB/HF-MINDO/3 calculations are close to zero, while those obtained with MNDO and AM1 are similar (0.022 and 0.028 meV, respectively). The differences between the results obtained with the various parametrizations can be directly interpreted in terms of differences in the atomic charge density distributions and the resulting quadrupole moments (Table II). Namely, while AM1, PM3, and, to a lesser degree, MNDO provide tensorial components of the ground-state quadrupole that are in good agreement with ab initio and experimental values,[24] the MINDO/3 values differ significantly. This discrepancy can be traced back to the method-dependent description of the ionicity of the C-H bonds: While AM1, PM3, and MNDO yield a charge distribution with the expected polarization (negative partial charges on C and positive ones on H), the MINDO/3 partial charges are much smaller and, in some cases, even of opposite signs (with negative partial charges on the hydrogens, see Table I).

We now move to the 2D and 3D clusters. As observed for 1D clusters, the molecular electrostatic energies obtained using MINDO/3 are 1 order of magnitude higher than the corresponding AM1 values (Fig. S2): The electrostatic energy per molecule, E_{el}/N, extrapolated to an infinite monolayer is about 0.3 eV at the AM1 level, while it amounts to 1.9 eV for MINDO/3; the corresponding 3D values are ~0.3 eV (AM1) and ~2.1 eV (MINDO/3). In addition, while a negligible change in electrostatic energy when going from the neutral to the charged 2D/3D clusters is predicted from MINDO/3 calculations, the effect is more pronounced at the AM1 level.

It should be stressed that $S^+=E_{el}^+-E_{el}$ arises primarily from the interactions between the excess charge on the fragment ion and the quadrupole moment of the neutral molecules (though our calculations include all multipolar interactions in both the neutral and charged stacks). Using a classical submolecular approach and experimental polarizability and quadrupole tensor components, Verlaak and Heremans estimated a charge-quadrupole interaction of −0.44 and −0.26 eV in 2D and 3D crystals, respectively.[26] The AM1 electrostatic energies from Fig. 3 of about −0.33 eV (for 2D clusters) and −0.13 eV (for 3D clusters) are consistent with the corresponding classical values, yet slightly smaller. That the MINDO/3 values (close to zero in both 2D and 3D clusters) are completely off is not really surprising, as this method provides a poor description of the anthracene quadrupolar tensor (*vide supra*).

B. Polarization energies

The dynamic polarization energy per molecular unit, as calculated at the VB/HF-AM1 and VB/HF-MINDO/3 levels

TABLE II. Principal components of the polarizability (in Å^3) and quadrupole moment (in D Å) of the anthracene molecule in its crystal geometry, as calculated using various semiempirical and *ab initio* schemes. The long (L), medium (M), and normal (N) axes are defined by the D_{2h} symmetry.

	Quadrupole moment			Polarizability			
	Θ_{LL}	Θ_{MM}	Θ_{NN}	α_{LL}	α_{MM}	α_{NN}	α_{LL}/α_{NN}
MINDO/3	−0.62	−0.44	1.06	34.53	19.11	3.56	9.71
MNDO	4.16	2.56	−6.72	35.56	19.41	2.67	13.33
AM1	8.53	5.55	−14.08	35.41	19.41	2.96	11.95
PM3	6.54	4.52	−11.08	34.38	18.67	3.11	11.05
HF/STO-3G	2.84	2.14	−4.98	24.89	13.63	1.93	12.92
HF/6-31G	6.56	5.72	−12.28	34.53	19.71	5.78	5.97
HF/6-311G*	7.23	6.19	−13.42	36.30	20.45	8.45	4.30
HF/6-311++G**	6.71	6.20	−12.91	38.08	21.49	12.15	3.13
B3LYP/6-311G*	6.28	5.34	−11.62	39.12	21.04	8.30	4.71
B3LYP/6-311++G**	5.74	5.30	−11.04	40.90	22.23	12.00	3.41
Reference values	7.94[a]	10.39[a]	−18.33[a]	35.23[b]	25.62[b]	15.21[b]	2.32[b]

[a]Reference 24.
[b]Reference 25.

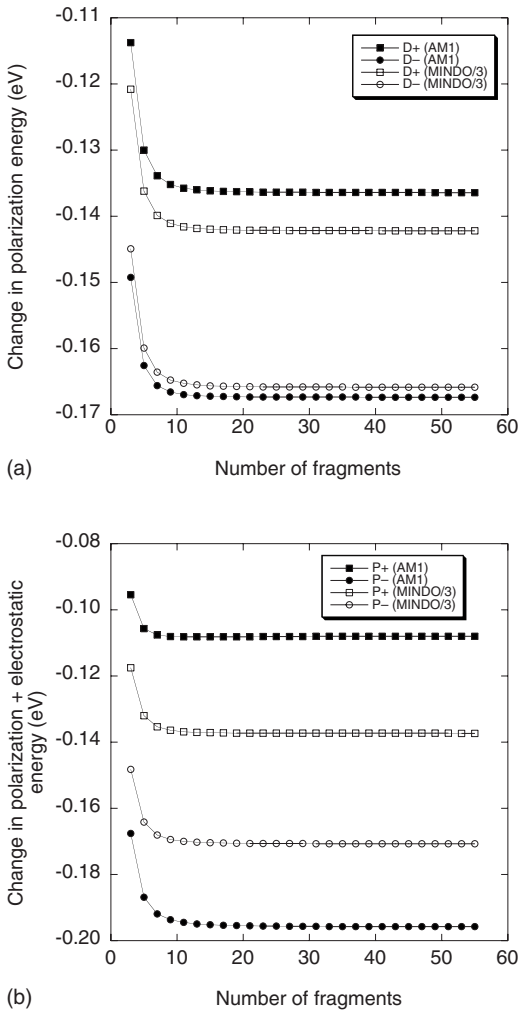

FIG. 4. (a) Evolution with cluster size of $D^+=E^+_{\mathrm{pol}}-E_{\mathrm{pol}}$ and $D^-=E^-_{\mathrm{pol}}-E_{\mathrm{pol}}$ (in eV), as calculated at the VB/HF-AM1 and VB/HF-MINDO/3 levels in 1D clusters. (b) Same for $P^+=(E^+_{\mathrm{pol}}+E^+_{\mathrm{el}})-(E_{\mathrm{pol}}+E_{\mathrm{el}})$ and $P^-=(E^-_{\mathrm{pol}}+E^-_{\mathrm{el}})-(E_{\mathrm{pol}}+E_{\mathrm{el}})$.

for neutral parallel stacks, remains close to zero (less than 1 meV) for all N [Figs. S3(a) S3(b)]. Calculations performed using the other parametrizations give very similar results and are not discussed further. These results indicate that the orbitals of a given fragment are weakly affected by their environment, which is not surprising in view of the small partial atomic charges in the anthracene molecule. This also reflects the large distance between fragments in the anthracene parallel stacks. As a matter of fact, when considering HB clusters where the intermolecular distances are smaller, the polarization energy per molecule is slightly higher and reaches ~ -2 meV in the infinite chain limit using AM1. Not surprisingly, the polarization energy per molecule increases when an excess charge is added on the central fragment (Fig. S3). It saturates in the parallel (HB) aggregates around -3 (-5) meV for both positively and negatively charged clusters whatever the parametrization.

The evolution with cluster size of the change in dynamic polarization energy for positive (D^+) and negative (D^-) charges, is illustrated in Fig. 4(a) in the case of parallel stacks. We recall that D^+ and D^- correspond to the difference in energy associated with electronic relaxation of charged and neutral clusters.

For the sake of comparison, the overall difference in dynamic polarization and electrostatic energy upon addition of a positive and negative charge in 1D clusters, i.e., $P^+=S^+ +D^+$ and $P^-=S^-+D^-$, respectively, is also reported [Fig. 4(b)]. These are the relevant quantities when dealing with hole and electron transport, as they provide a direct measure of the change in intermolecular energy in the presence of an excess positive or negative charge. It is interesting to note the asymmetry in stabilization energy for a positive vs a negative charge, especially pronounced at the AM1 level, with $|D^-|>|D^+|$. This can be understood on the basis of the charge distribution pattern based on a united atom approach (Table I). In the AM1 neutral ground state, the CH units bear positive partial charges that are compensated by negative charges on the H-free C atoms. While this effect is reinforced in the molecular cation, where the same pattern is observed, the partial charges are distributed with the opposite pattern in the anion. Hence, according to the AM1 calculations, there is a more pronounced repolarization of the electronic cloud

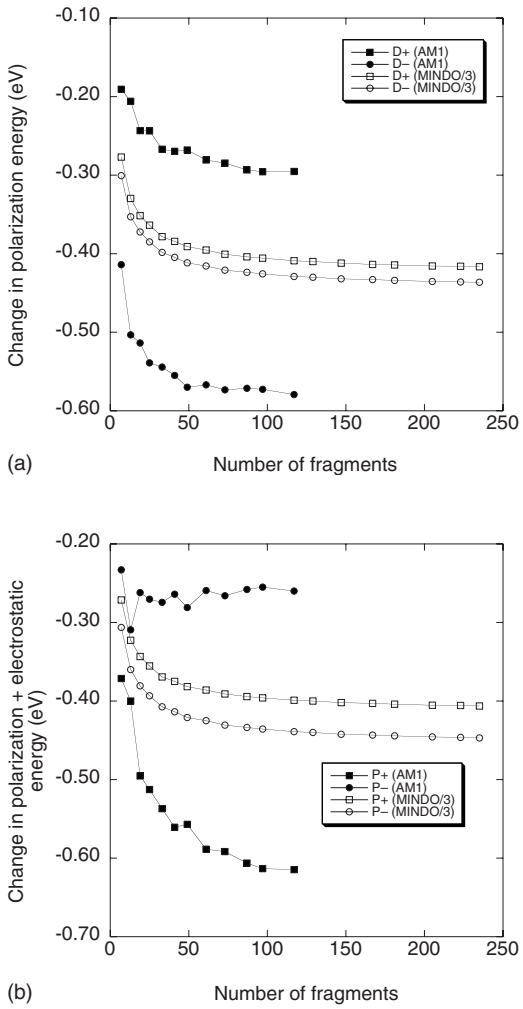

FIG. 5. (a) Evolution with cluster size of $D^+=E^+_{\mathrm{pol}}-E_{\mathrm{pol}}$ and $D^-=E^-_{\mathrm{pol}}-E_{\mathrm{pol}}$ (in eV), as calculated at the VB/HF-AM1 and VB/HF-MINDO/3 levels in 2D clusters. (b) Same for $P^+=(E^+_{\mathrm{pol}}+E^+_{\mathrm{el}})-(E_{\mathrm{pol}}+E_{\mathrm{el}})$ and $P^-=(E^-_{\mathrm{pol}}+E^-_{\mathrm{el}})-(E_{\mathrm{pol}}+E_{\mathrm{el}})$.

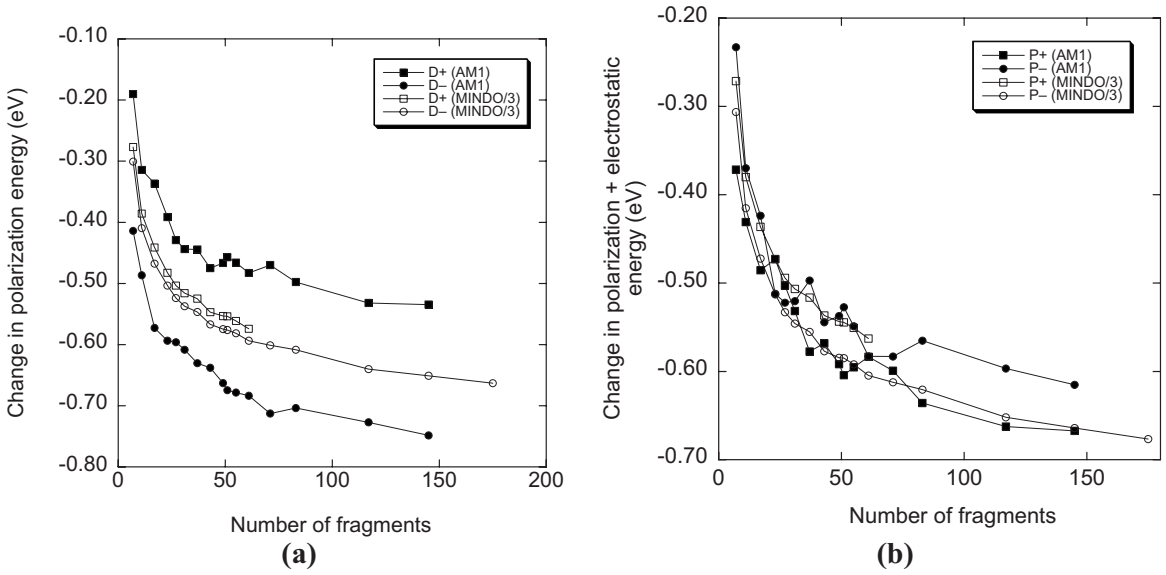

FIG. 6. (a) Evolution with cluster size of $D^+=E^+_{\mathrm{pol}}-E_{\mathrm{pol}}$ and $D^-=E^-_{\mathrm{pol}}-E_{\mathrm{pol}}$ (in eV), as calculated at the VB/HF-AM1 and VB/HF-MINDO/3 levels in 3D clusters. (b) Same for $P^+=(E^+_{\mathrm{pol}}+E^+_{\mathrm{el}})-(E_{\mathrm{pol}}+E_{\mathrm{el}})$ and $P^-=(E^-_{\mathrm{pol}}+E^-_{\mathrm{el}})-(E_{\mathrm{pol}}+E_{\mathrm{el}})$.

when adding an excess electron. As a matter of fact, the asymmetry in D^+ vs D^- values is significantly reduced at the MINDO/3 level, owing to a smaller ionic character in the neutral form.

The polarization energy per molecule in the 2D clusters follows the same evolution with the number of anthracene molecules as that found in 1D stacks (Fig. S4). As in the 1D case, the change in dynamic electronic polarization energy between the neutral and anionic clusters, D^-, is larger in absolute values than the corresponding energy difference for the cationic clusters, D^+ [Fig. 5(a)]. For the same reasons as described above, this effect is much more pronounced at the AM1 level. Yet, note that the total change in intermolecular energy, i.e. the sum over electrostatic and dynamic polarization contributions, shows the opposite trend with $|P^+|>|P^-|$ [Fig. 5(b)]. This trend, which results from the fact that electrostatic and polarization terms add up in the positively charged case but have opposite signs in the negatively charged clusters, is consistent with the generally accepted assumption that cations are more stabilized than anions when going from the gas phase to the bulk.[27] It should also be kept in mind that the quadrupolar interactions involved in $S^{+(-)}$ actually depend on the shape of the cluster, which might somehow affect the conclusions above.[28]

The AM1 dynamic polarization energy per molecule [Fig. S5(a)] as extrapolated for neutral infinite 3D clusters (~ -5 meV), is in close agreement with the value of −2.8 meV calculated by Tsiper and Soos on the basis of an atomistic classical model.[28] As expected, the corresponding MINDO/3 values [Fig. S5(b)] are much smaller. The 3D results follow qualitatively the 2D ones, with changes in dynamic polarization energy for positive and negative charges computed at the AM1 level bracketing the corresponding MINDO/3 values [see Fig. 6(a)]. Inclusion of electrostatic contributions yields a more chaotic evolution of the overall change in intermolecular energy with cluster size and $|P^+|>|P^-|$ from AM1 calculations. The latter result is consistent with the classical polarization energies obtained by summing over the charge-induced dipole and charge-quadrupole interactions.[28]

Finally, we portray in Fig. 7 the evolution with the number of fragments of the sum P^++P^- in parallel 1D, 2D, and 3D clusters. Because charge-quadrupole interactions for positive and negative charges cancel out, smoother size-dependent curves are obtained and allow for extrapolation to infinite size aggregates. As expected, P^++P^- increases with dimensionality from ~ -0.31 eV for 1D to ~ -0.92 eV for 2D and ~ -1.66 eV for 3D. Strikingly similar results are obtained from the MINDO/3 calculations that correctly reproduce the reorganization of the electronic cloud in the presence of an excess charge despite failing completely to describe the charge-quadrupole interactions.

Figure 7(c) shows the linear dependence of P^++P^- with R^{-1} in the 3D spherical clusters, from which extrapolated values of −1.66 and −1.70 eV are extracted at the AM1 and MINDO/3 levels, respectively. These polarization energies are comparable to the values calculated by Tsiper and Soos[28] using a mixed quantum/classical approach and a decomposition of the total molecular polarizability into two contributions,

$$\alpha_{\mathrm{ab}}=\alpha^C+\tilde{\alpha},$$

where α^C is the "charge only" molecular component that measures the charge redistribution among atoms in the external potential and $\tilde{\alpha}$ is the purely atomic component scaling linearly with the number of valence electrons. Our evaluations of P^++P^- agree with the charge only ($\tilde{\alpha}=0$) value of about −1.8 eV obtained by Tsiper and Soos, assuming that the electronic polarization is due entirely to charge redistribution. However, they are smaller than the total value of −2.204 eV obtained at the classical level when accounting for the atomic contributions to the polarizability. Using a submolecular classical approach, Verlaak and Heremans reported a yet higher value of −2.64 eV for P^++P^- in the bulk

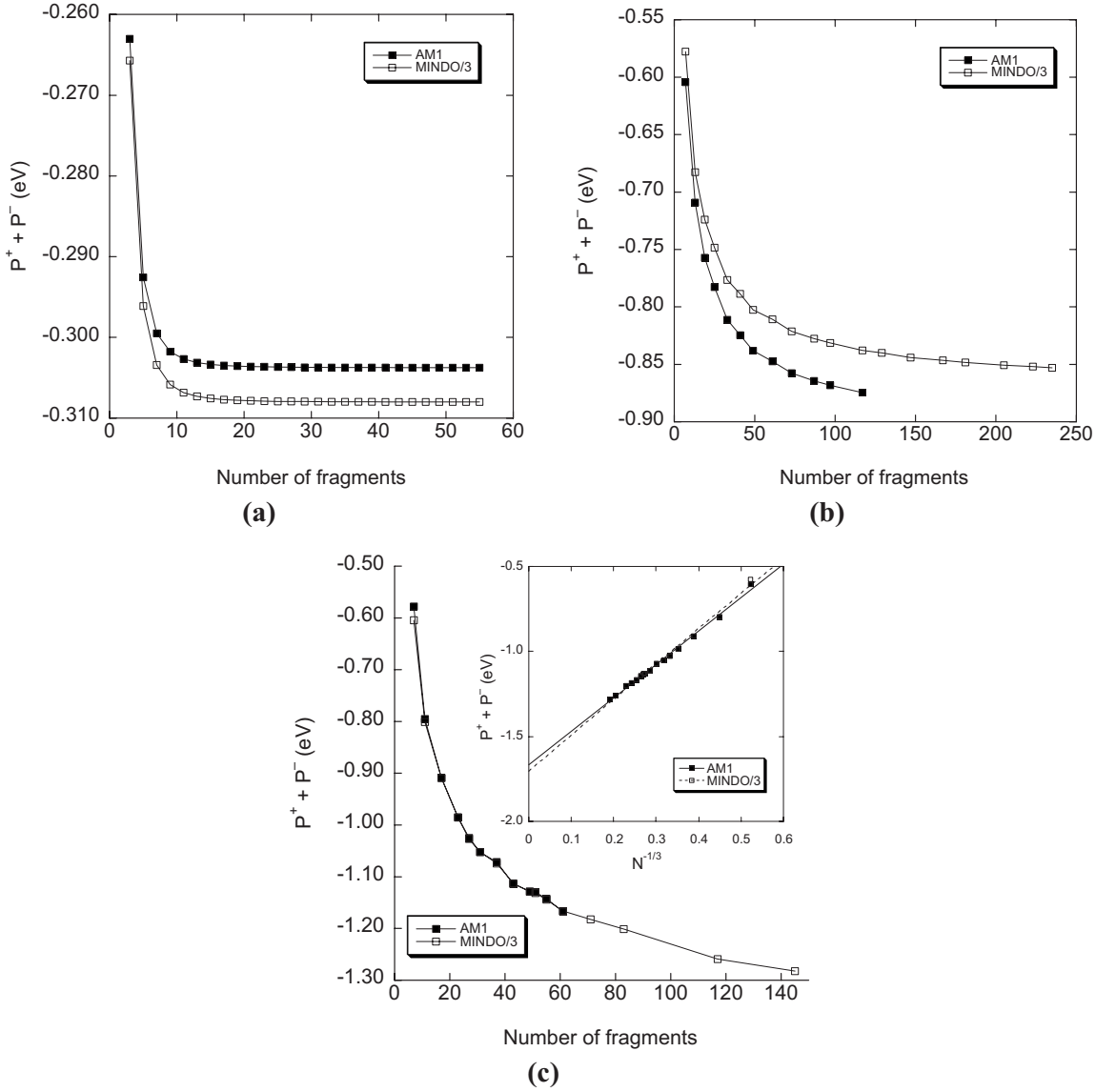

FIG. 7. Evolution with cluster size of $P^+ + P^-$, as calculated at the VB/HF-AM1 and VB/HF-MINDO/3 levels in (a) 1D, (b) 2D, and (c) 3D clusters. Inset of (c): Evolution of $P^+ + P^-$ with $N^{-1/3}$. Straight lines are linear fits.

anthracene crystal[26] [the authors actually reported a value of −1.32 eV for charge-induced dipole interactions ($E_{\text{q-Id}}$); assuming a perfect electron-hole symmetry, charge-quadrupole interactions cancel out and $P^+ + P^- = 2E_{\text{q-Id}}$]. The reason for the underestimated VB/HF polarization energies can be traced back to the minimal valence basis set used in the semiempirical schemes, which yields polarizability components normal to the molecular planes that are underestimated compared to the results obtained with *ab initio* calculations using large basis sets. For the sake of illustration, we compare in Table II the principal components of the α tensor for the anthracene molecule, as calculated within various semiempirical and *ab initio* schemes. The corresponding experimental values are also reported. Not surprisingly, the need for extended and diffuse basis sets for a proper description of α clearly shows up from the table: Although the in-plane components are quite well reproduced by all theoretical schemes, the underestimation of the out-of-plane component is severe when using reduced basis sets and *a fortiori* semiempirical Hamiltonians.

On the other hand, it is also obvious that such high-level *ab initio* computational schemes are prohibitive so that semiempirical Hamiltonians remain the unique way for a full quantum-chemical treatment of large systems. Additionally, the mere application of a VB scheme is questionable when using diffuse atomic orbitals. A possible solution to deal with the minimal basis set problem inherent to semiempirical schemes would be to use semiempirical parameters fitted to reproduce the molecular polarizabilities provided by high-level *ab initio* calculations. In order to test this idea, we have performed a finite-field calculation of α for the isolated anthracene molecule by reducing the Slater exponents for the $2s$ and $2p$ orbitals of the C and H atoms by a factor of 1.8. The diagonal components of the polarizability obtained using this reparametrized AM1 method are (in Å^3): $\alpha_{LL}=38.2$, $\alpha_{MM}=22.8$, and $\alpha_{NN}=8.2$; the ratio α_{LL}/α_{NN} is now equal to

TABLE III. Hopping matrix elements (in meV) between the central fragment M (see Fig. 1) of a 3D anthracene cluster (R =11 Å) and its first neighbors X within the crystal (a,b) plane.

	$M^+ + X \rightarrow M + X^+$		$M^- + X \rightarrow M + X^-$	
$M=(0,0,0)$	AM1	MINDO/3	AM1	MINDO/3
X=(1,0,0)	2.9	3.4	0.4	0.51
X=(0,1,0)	10.7	12.8	7.2	8.04
$X=(1/2,1/2,0)$	9.0	10.4	12.7	13.80

4.69, which is very close to the reference values. Moreover, using this modified AM1 parametrization, the extrapolated value of $P^+ + P^-$ for an infinite crystal yields 1.94 eV, which is in better agreement with the previously reported evaluations. Although further work is needed, this preliminary test proves that it is, in principle, possible to yield quantitative estimates of polarization effects on charge carriers by simply tuning the semiempirical parameters while keeping the description of the wave function based on a minimal valence basis set. Another option would be to use Clementi's orbitals, i.e., contracted Slater orbitals instead of single Slater orbitals,[29] as this may improve the long-range part of the molecular wave functions and, hence, the description of both the polarization energies and the transfer integrals, *vide infra*. Further work is in progress along that line.

IV. HOPPING MATRIX ELEMENTS

A. Electron and hole transfer: Anisotropy effects

Hopping matrix elements between adjacent fragments were calculated from Eq. (5) on the basis of many-body wave functions provided by various semiempirical parametrizations. A detailed analysis of the parametrization effects is provided in appendix. We report in Table III the nearest neighbor couplings for hole and electron transport, as calculated between "solvated" fragments, i.e., embedded in a "spherical" 3D cluster, at the AM1 and MINDO/3 levels.

These results show that the transfer integrals strongly depend on the relative orientation of the interacting fragments. In addition, the degree of anisotropy differs for holes and electrons: Along the b direction, hole transfer interactions are larger than their electron counterparts, while the opposite is true for the coupling between the two HB molecules of the unit cell (i.e., along the diagonal direction). Note that the hopping matrix elements computed for anthracene are found to be 1 order of magnitude smaller than those calculated within the same framework in other crystals, such as organic conductors derived from Bechgaard salts.[10] This is related to the much larger intermolecular distances between fragments in the anthracene crystal (5.99 Å along the parallel stacking direction) compared to the typical interchain distance of 3.5 Å in stacks of, e.g., tetrathiofulvalene derivatives. We also stress that the calculated transfer integrals provided by AM1 and MINDO/3 are much smaller (by up to 1 order of magnitude) compared to the corresponding values obtained either at the *ab initio* level as well as with the semiempirical INDO technique,[30] which are generally found to be in good quantitative agreement[3]). A more detailed discussion of the evaluation of the transfer integrals using methods based on the NDDO approximation is presented in the Appendices.

TABLE IV. Hopping matrix elements (in meV) for hole and electron transfer between isolated dimers in the various crystalline stacking directions, as calculated at the VB/HF-AM1 level, using frozen (1) and relaxed (2) molecular orbitals. The molecule labels are shown in Fig. 1.

	$M^+ + X \rightarrow M + X^+$		$M^- + X \rightarrow M + X^-$	
$M=(0,0,0)$	(1)	(2)	(1)	(2)
X=(1,0,0)	3.3	2.5 (−24%)	0.5	0.5 (−0%)
X=(0,1,0)	10.8	9.3 (−14%)	6.6	6.4 (−3%)
$X=(1/2,1/2,0)$	9.8	7.5 (−23%)	12.23	11.68 (−4%)

B. Polarization effects

Table IV collects the nondiagonal matrix elements for hole and electron transfer between isolated dimers in the various crystalline stacking directions, as computed prior and after relaxation of the electronic cloud. The comparison between these values provides a direct assessment for the influence of electronic polarization effects on charge-transfer integrals. As expected, the *in situ* optimization of the MOs induces relatively small changes in the electronic couplings due to the negligible overlap between the fragments. Yet, for hole transport, a systematic decrease of the coupling matrix elements, which can reach up to 24% of the bare values is predicted. This decrease is much smaller in the case of electron transport. In addition, this correction is sensitive to the packing direction and might therefore somewhat affect the anisotropy in the charge transport properties of the crystal.

The same calculations have been extended to spherical 3D clusters of radius R=11 Å. The results reported in the second and third columns of Table V are consistent with those obtained in the dimer case: The hopping matrix elements between two fragments embedded in their environment, but using the unrelaxed MOs, are, in all cases, larger than the values computed after full electronic relaxation. On a quantitative level, the orbital relaxation of all fragments in the

TABLE V. Hopping matrix elements (in meV) for hole transfer between the central fragment in a 3D anthracene cluster (R =11 Å) and its nearest neighbors, as calculated at the VB/HF-AM1 level. [(1) Fragments with frozen molecular orbitals, (2) fragments with relaxed MOs [Eq. (5)], (3) HOMO contribution to the hopping matrix elements, and (4) one-electron integral between the HOMOs of the two fragments.] The molecule labels are shown in Fig. 1.

	(1)	(2)	(3)	(4)
X=(1,0,0)	3.3	2.9 (−12%)	2.8	2.7
X=(0,1,0)	11.2	10.7 (−4%)	9.6	10.2
$X=(1/2,1/2,0)$	10.1	9.0 (−11%)	8.1	8.6

cluster leads to a slightly smaller (compared to the dimer) lowering (by 4%–10%) of the coupling matrix elements depending on the stacking direction. This result suggests that, despite being of relatively small amplitude in the case of anthracene, polarization effects on the electronic couplings might not be negligible in crystals with stronger van der Waals interactions.

Finally, a comparison between the third and fourth columns of Table V demonstrates that the coupling between the fragment HOMOs contributes the most to the total matrix elements, the contributions from deeper occupied molecular orbitals being small although not negligible. It is also clear from the values in the fifth column that the bicentric one-electron integral between the HOMOs of the two fragments represents a good approximation of the total off-diagonal matrix element.

In their seminal work on charge-carrier mobilities in organic molecular solids, Glaeser and Berry predicted a significant (up to 40%–50%) reduction in the transfer integrals when accounting for polarization corrections,[27,31] while Petelenz estimated a smaller impact of the environment (15%).[32] More recently, Bussac *et al.* showed that inclusion of electronic polarization effects results in a renormalization of the transfer integrals that substantially decreases their values (by about 17% in the case of anthracene) compared to the bare case.[33] Our results are consistent with these earlier studies and suggest that dressing effects induced by electronic polarization significantly influence the amplitude of the electronic couplings in the hopping regime as well as their anisotropy.

C. Comparison with transfer integrals evaluated from the "dimer-splitting" approximation

A widely used method for evaluating transfer integrals relies on the avoided crossing of two eigenstates that result from the mixing between donor (D) and acceptor (A) valence bond states. When the A and D states are degenerate and orthogonal, the coupling matrix element H_{DA} is equal to half the energy difference between the two eigenstates in the transition state geometry. Within the Hartree–Fock approximation, the H_{DA} term related to hole transfer is usually approximated by using the "dimer energy splitting" method, i.e., by taking half the splitting between the two (adiabatic) highest occupied molecular orbitals in the neutral dimer.[34] In a similar way, the electronic couplings mediating the transfer of an excess electron are evaluated from the difference in the energies of the lowest two unoccupied (one-electron) MOs of the neutral dimer. In contrast, the calculation of the VB/HF coupling matrix elements (i) relies on the explicit definition of the VB charge-transfer states in the framework of local monomer orbitals, (ii) accounts for the presence of the excess charge, and (iii) is based on a many-body description of the wave functions.

The electronic couplings for an isolated dimer comprising two anthracene molecules packed along the b axis calculated using the two approaches are compared in Table VI. Taking into account the very different approaches, the agreement is quite satisfactory and demonstrates that, in this particular case, the dimer-splitting approach constitutes a simple and effective method to calculate the transfer matrix elements.

TABLE VI. Comparison between hopping matrix elements (in meV) calculated with the VB/HF and the dimer-splitting approaches.

	$M^+ + X \rightarrow M + X^+$		$M^- + X \rightarrow M + X^-$	
	VB/HF	Dimer splitting	VB/HF	Dimer splitting
AM1	9.29	11.94	6.43	8.15
MNDO	6.24	8.00	4.41	5.69
PM3	5.28	6.84	4.10	5.15
MINDO/3	13.02	14.01	8.52	9.07

However, the dimer-splitting approximation is, strictly speaking, applicable only to symmetrical arrangements where the atomic coordinates of the involved molecules can be deduced from each other via symmetry operations, i.e., for equivalent molecules in a crystal. Nonequivalent molecules, even if they are chemically identical, polarize each other differently, leading to a site energy mismatch $E_D \neq E_A$. In this case, the energy-splitting approach can drastically overestimate the transfer integrals by introducing a significant contribution from the polarization-induced site energy difference. This was demonstrated recently by Valeev *et al.*[35] who calculated the effect of electronic polarization on charge-transfer terms in ethylene and pentacene dimers with a procedure using localized monomer orbitals, similar to that previously used by Siebbeles and co-workers to evaluate the hole transfer terms in nucleoside stacks[36] and in columnar stacked triphenylenes.[37]

The difference between the VB/HF procedure and the dimer-splitting approximation is further illustrated for hole and electron transfer in anthracene in Figs. 8(a) and 8(b) reporting the evolution of the transfer integrals between parallel molecules (Fig. 9) as a function of the translation along their long axis. For both hole and electron transfer, the electronic couplings calculated from VB/HF and the dimer-splitting approximation are quite similar. The small differences arise from the self-consistent optimization of the MOs in the dimer calculation, which produces combinations of fragment MOs that are not strictly equivalent to the VB/HF local MOs, as well as from the fact that the VB/HF local MOs of the two VB configurations are affected by the net charge of the fragments while the energy splitting approach is based on the neutral dimer.

In contrast, when considering the rotation of one monomer around the long axis of the other (which is typical of an HB-type stacking, see Fig. 10), the dimer-splitting approximation drastically overestimates the hopping integrals [see Figs. 8(c) and 8(d)]. This overestimation, whose amplitude increases with the rotational angle, is maximal in the "face-to-edge" structure, where the largest contribution to the splitting of the D/A states arises from electrostatic effects. These spurious effects might be even more pronounced when using diffuse orbitals within an *ab initio* formalism. To circumvent this problem, several authors have proposed to apply a homogeneous electric field from the donor to the acceptor[38] in order to equalize the energy of the D and A states, with,

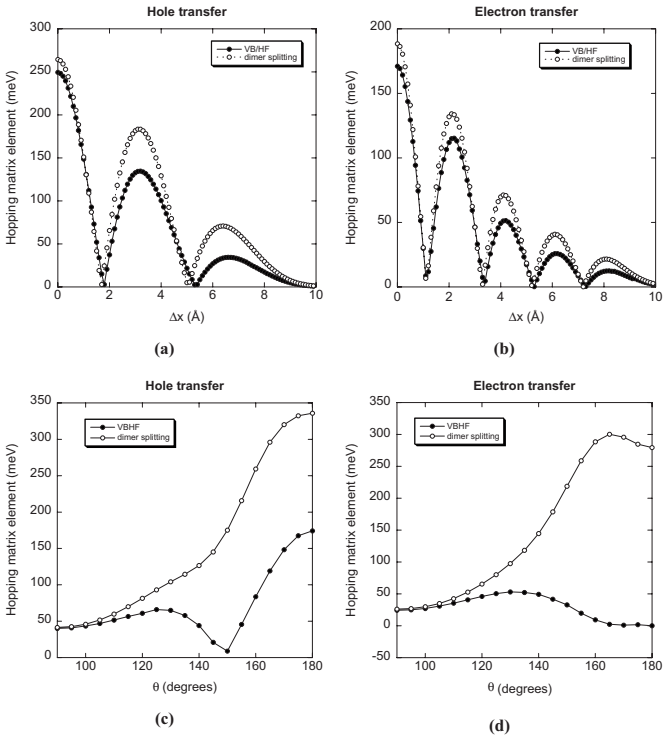

FIG. 8. Hopping matrix element in the anthracene dimer, as calculated using the VB/HF-AM1 and dimer splitting methods. (a) and (b): evolution as a function of the translation along the long axis [see Fig. 9]. (c) and (d): evolution as a function of the tilt angle [see Fig. 10].

nevertheless, the risk to generate an arbitrary polarization of the electronic cloud.

V. CONCLUDING REMARKS

A fragment orbital-based VB/HF model has been presented to evaluate the polarization energies and the coupling matrix elements among adjacent molecules embedded in a polarizable medium and applied to the anthracene single crystal. Such parameters are highly relevant for the modeling of charge transport processes in molecular crystals and can be injected in transfer rate expressions, derived, in particular, from the Marcus theory, to yield hopping rates in a completely consistent approach and in the absence of any adjustable parameter. The combination of the VB/HF model with semiempirical Hamiltonians allows us to deal with extended systems, with an explicit account of long-range and nonadditive effects within a complete quantum treatment of valence shell electrons, as required to evaluate reliably bulk properties from finite molecular aggregates.

However, this series of test calculations applied to anthracene clusters also highlights the limitations of the standard semiempirical schemes. Due to the minimal valence basis set used in these models, the out-of-plane molecular polarizablity component is underestimated compared to the in-plane components, leading to an underestimation of the polarization energies. The lack of flexibility of the wave function also rationalizes why the transfer integrals between two distinct fragments are less sensitive to the molecular environment than those obtained from *ab initio* calculations with extended basis sets. Moreover, the coupling matrix elements evaluated within the NDDO approximation also suffers from an inherent deficiency due to the neglect of two-electron interactions (see Appendix A).

These limitations could be bypassed through an *ab initio* derivation of the VB/HF model. However, such methods would suffer from other drawbacks, namely, the difficulty to deal with large systems, which is the interest of simplified semiempirical schemes. Moreover, the strong orthogonality condition allowing for a strict partitioning of electron groups, which is natural within NDDO schemes, would not be fulfilled within an *ab initio* context using extended and overlapping basis sets.

A more subtle way to reach a quantitative agreement with reference values would consist in introducing diffuse orbitals in the semiempirical scheme. However, beyond the fact that a complete reoptimization of the full set of parameters would be needed, this would also reduce the simplicity of the model. Preliminary calculations performed with modified NDDO semiempirical parameters have demonstrated that it is possible to correct the underestimation of the out-of-plane polarizability component without the need for split valence shell orbitals. This approach seems to be the most promising for forthcoming developments of the VB/HF scheme in order to achieve a more quantitative description of polarization effects in organic crystals.

When applied to anthracene clusters, the present calculations recover a large fraction of the electronic polarization energy associated with a localized charge, in comparison to experimental values or results obtained from submolecular or atomistic classical calculations. They further indicate that the dressing of the charge carriers by the polarization cloud results in a decrease (by up to 20%) of the hopping matrix elements. Interesting applications of our VB/HF approach include the extension to more disordered structures and the

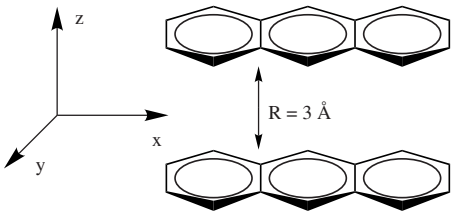

FIG. 9. Parallel anthracene dimer. The evolution of the hopping terms as a function of the translation along the x axis is illustrated in Fig. 8(a) and 8(b).

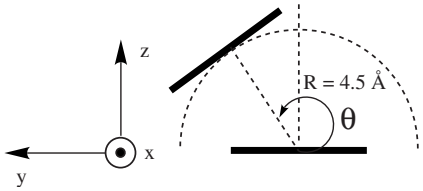

FIG. 10. From the face-to-face (θ=0°) to the face-to-edge (θ=90°) dimer structure. The evolution of the hopping terms as a function of θ is illustrated in Fig. 8(c) and 8(d).

investigation of the impact of the lattice vibrations on the amplitude of the polarization energies and coupling matrix elements. These studies are in progress.

ACKNOWLEDGMENTS

This work has benefited from the European Commission STREP project MODECOM (NMP-CT-2006-016434), a Tournesol scientific cooperation established and supported by the Centre National de la Recherche Scientifique (CNRS), the Belgian National Fund for Scientific Research (FNRS), and the Commissariat Général aux Relations Internationales (CGRI) de la Communauté Wallonie-Bruxelles. F.C. and L.D. thank S. Ramasesha for helpful discussions. D.B. thanks the University Bordeaux I for his visiting scientist position. Calculations were carried out on main frame computers of the "M3PEC-MESOCENTRE" of the University Bordeaux I financed by the Conseil Régional d'Aquitaine and the French Ministry of Research and Technology, as well as on the Interuniversity Scientific Calculation Facility (ISCF) installed at the Facultés Universitaires Notre-Dame de la Paix (Namur, Belgium) for which the authors gratefully acknowledge the financial support of the FNRS-FRFC. J.C. and D.B. are FNRS Research Associate and Research Director, respectively.

APPENDIX A: FURTHER DISCUSSION ON THE SEMIEMPIRICAL EVALUATION OF THE COUPLING MATRIX ELEMENTS

Suppose we have a pair of molecules A-B. From Eq. (3), the coupling matrix element associated with the transfer of one hole implies the two VB configurations $\kappa=|AB^+\rangle$ and $\eta=|A^+B\rangle$ and is expressed as

$$H_{\kappa\eta}=\langle AB^+|\hat{H}|A^+B\rangle. \tag{A1}$$

This term can be separated in its one- and two-electron parts,

$$H_{\kappa\eta}=\langle AB^+|\hat{h}|A^+B\rangle+\langle AB^+|\hat{g}|A^+B\rangle, \tag{A2}$$

where $\hat{h}$ and $\hat{g}$ are the one- and two-electron parts of the total Hamiltonian operator $\hat{H}$,

$$\hat{h}=\sum_{\nu}\left(-\frac{1}{2}\Delta_{\nu}-\sum_{Q}\frac{Z_Q}{R_{Q\nu}}\right),\quad \hat{g}=\frac{1}{2}\sum_{\nu\mu}\frac{1}{r_{\nu\mu}}. \tag{A3}$$

In the one-electron operator, the sum over Q runs over all the nuclei of the two fragments. As discussed above [see Eq. (5)], the nonorthogonality of the fragment MOs involved in the Slater determinants associated with the two charge-transfer states imposes that the coupling terms follow Löwdin' rules. For the one-electron part, one has

$$\langle AB^+|\hat{h}|A^+B\rangle=\sum_{R,S}\sum_{i,j}(-1)^{i+j}\det(S^{\kappa\eta}_{i,j})\cdot\langle\varphi^R_{\kappa,i}|\hat{h}|\varphi^S_{\eta,j}\rangle, \tag{A4}$$

where $\det(S^{\kappa\eta}_{i,j})$ is the cofactor of the overlap matrix $\mathbf{S}^{\kappa\eta}$, i.e., the determinant of the matrix obtained after removing the line and column that contain the term $\langle\varphi^R_{\kappa,i}|\varphi^S_{\eta,j}\rangle$. Because of the locality constraint of the MOs, the overlap matrix $\mathbf{S}^{\kappa\eta}$ contains two rectangular blocks, as illustrated in Fig. 11.

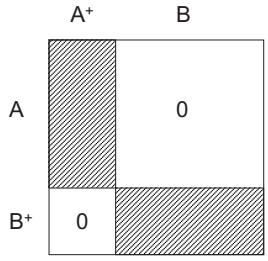

FIG. 11. Overlap matrix between the fragments MOs in the two VB configurations $\kappa=|AB^+\rangle$ and $\eta=|A^+B\rangle$. The dashed blocks contain nonzero elements, while the overlap is zero in the white areas.

Because of the peculiar form of the $\mathbf{S}^{\kappa\eta}$ matrix, the only nonzero terms in Eq. (A4) are obtained when $R=A$ and $S=B$, i.e., when the MOs $\varphi^R_{\kappa,i}$ and $\varphi^S_{\eta,j}$ belong to the acceptor and the donor site, respectively.

The two-electron part of the coupling term is expressed as

$$\langle AB^+|\hat{g}|A^+B\rangle=\sum_{i}\sum_{k\neq i}\sum_{j}\sum_{l\neq j}(-1)^{i+k+j+l}\varepsilon_{ik}\varepsilon_{jl}\det(S^{\kappa\eta}_{i,k,j,l})\times\langle\varphi^R_{\kappa,i}\varphi^{R'}_{\kappa,k}|\hat{g}|\varphi^S_{\eta,j}\varphi^{S'}_{\eta,l}\rangle, \tag{A5}$$

assuming an implicit summation over the molecules R, R', S, and S'. $\varepsilon_{ik}=1$ $(i<k)$, $\varepsilon_{ik}=-1$ $(i>k)$, $\varepsilon_{jl}=1$ $(j<l)$, and $\varepsilon_{jl}=-1$ $(j>l)$. $\det(\mathbf{S}^{\kappa\eta}_{i,k,j,l})$ is the determinant of the overlap matrix obtained after deleting the lines and columns containing the terms $\langle\varphi^R_{\kappa,i}|\varphi^S_{\eta,j}\rangle$ and $\langle\varphi^{R'}_{\kappa,k}|\varphi^{S'}_{\eta,l}\rangle$. For the same reason as above, nonzero terms only arise when $R=A$ and $S=B$, and $R'=S'$. The expansion of the fragment MOs over the atomic orbital (AO) basis gives

$$\langle\varphi^A_{\kappa,i}\varphi^M_{\kappa,k}|\hat{g}|\varphi^B_{\eta,j}\varphi^M_{\eta,l}\rangle=\sum_{p,q,r,s}C^{\kappa}_{pi}C^{\kappa}_{kr}C^{\eta}_{jq}C^{\eta}_{ls}\langle\chi^A_p\chi^M_r|\hat{g}|\chi^B_q\chi^M_s\rangle, \tag{A6}$$

where $M=A$ or B. The two-electron integrals in Eq. (A6) are neglected in the NDDO approximation, so that the two-electron part of the coupling term is strictly zero within a semiempirical framework.

Then, within an NDDO implementation of the VB/HF model, only the interactions between the electrons of a fragment and the nuclei of the other are explicitly included in the expression of the coupling terms, and are not counterbalanced by the corresponding electron-electron repulsion. This purely monoelectronic character may thus induce an overestimation of the coupling terms. However, in the NDDO schemes, one-electron integrals are taken to be proportional to the overlap between the corresponding MOs and, thus, decrease exponentially with R (see Appendix B), which is intuitively expected for charge-transfer integrals. Note also that the two charge-transfer states $\kappa=|AB^+\rangle$ and $\eta=|A^+B\rangle$ are obtained independently by performing local mean-field procedures, so that the mutual polarization of the electronic clouds of A and B is implicitly taken into account (though it does not appear explicitly in the coupling term). Besides, the

TABLE VII. Hopping matrix elements (in meV) for hole and electron transport between isolated dimers stacked along the *b* crystalline axis, as calculated using various semiempirical parametrizations.

	Hole transport	Electron transport
AM1	9.29	6.43
MNDO	6.24	4.41
PM3	5.28	4.10
MINDO/3	13.02	8.52

representation of the AOs by a single Slater function is bound to underestimate the coupling terms at a large distance, so that the two effects tend to compensate each other, leading finally to qualitatively correct estimations of the coupling terms.

APPENDIX B: IMPACT OF THE SEMIEMPIRICAL PARAMETRIZATION ON THE COUPLING MATRIX ELEMENTS

The results reported in Table VII, as well as those presented in Sec. IV, reveal an overall strong sensitivity of the hopping matrix elements on the parametrization. The origin of such differences can be tracked back from the expression of the two-center one-electron transfer integrals between the HOMOs of fragments R and S,

$$\langle \varphi^R_{\kappa,i}|\hat{h}|\varphi^S_{\eta,j}\rangle = \sum_{p,q} C^{\kappa}_{pi} C^{\eta}_{qj} \langle \chi^R_p|\hat{h}|\chi^S_q\rangle = \sum_{p,q} C^{\kappa}_{pi} C^{\eta}_{qj} h_{pq}. \quad \text{(B1)}$$

The main difference between the various NDDO parametrizations arises from the atomic h_{pq} terms, which depend, in turn, on the overlap terms S_{pq} and on the semiempirical parameters,

$$\langle \chi^R_p|\hat{h}|\chi^S_q\rangle = \frac{1}{2}[\xi_{A\in R}(\chi_p) + \xi_{B\in S}(\chi_q)]S_{pq}. \quad \text{(B2)}$$

The $\xi_X(\chi)$ parameters, which depend on the nature of the atom X and its orbital χ, are determined using semiempirical criteria that significantly differ in the various parametrizations. In the anthracene fragments, the HOMOs are expanded only on the basis of the $2p_\pi$ orbitals of the carbon atoms, with $\xi_C(2p) = -7.7193$, -7.9341, and -9.8027 eV in AM1, MNDO, and PM3, respectively. In addition, the differences also originate from the parametrization of the overlap integrals in view of the different values of the Slater exponents for the $2p$ atomic orbitals: 1.6851 (AM1), 1.7875 (MNDO), and 1.8423 (PM3). The Slater exponents are larger with MNDO and PM3 than with AM1, yielding more compact atomic orbitals and, thus, smaller transfer integrals.

With the MINDO/3 model, the bicentric one-electron integrals between two AOs centered on atoms A and B are approximated by

$$\langle \chi^R_p|\hat{h}|\chi^S_q\rangle = \xi_{A,B}(I_{A\in R}(\chi_p) + I_{B\in S}(\chi_q))S_{pq}, \quad \text{(B3)}$$

where the resonance integral multiplier $\xi_{A,B}$ between two carbons is 0.419 907 and the valence state ionization potential $I_C(2p)$ amounts to -11.54 eV. One-electron integrals between $2p$ orbitals of distinct carbon atoms are then expressed as $h_{pq} = -9.6915 \times S_{pq}$. In addition, the Slater exponent used in the overlap S_{pq} is equal to 1.7096, thus yielding larger transfer integrals than those provided by the NDDO-based Hamiltonians.

*Corresponding authors.
†FAX: +33 5 4000 66 45; f.castet@ism.u-bordeaux1.fr
‡FAX: +32 65 37 38 61; david@averell.umh.ac.be

[1] See, for example, Chem. Rev. (Washington, D.C.) **107** (2007), special issue.
[2] W. Warta and N. Karl, Phys. Rev. B **32**, 1172 (1985).
[3] V. Coropceanu, J. Cornil, D. A. da Silva Filho, Y. Olivier, R. Silbey, and J. L. Brédas, Chem. Rev. (Washington, D.C.) **107**, 926 (2007).
[4] A. Troisi and G. Orlandi, Phys. Rev. Lett. **96**, 086601 (2006).
[5] M. Hultell and S. Stafström, Chem. Phys. Lett. **428**, 446 (2006).
[6] R. A. Marcus, Rev. Mod. Phys. **65**, 599 (1993).
[7] Y. Olivier, V. Lemaur, J. L. Bredas, and J. Cornil, J. Phys. Chem. A **110**, 6356 (2006).
[8] E. F. Valeev, V. Coropceanu, D. A. da Silva, S. Salman, and J. L. Bredas, J. Am. Chem. Soc. **128**, 9882 (2006); K. Senthilkumar, F. C. Grozema, F. M. Bickelhaupt, and L. D. A. Siebbeles, J. Chem. Phys. **119**, 9809 (2003).
[9] F. Castet, A. Fritsch, and L. Ducasse, J. Phys. I **6**, 583 (1996).
[10] F. Castet, L. Ducasse, and A. Fritsch, Chem. Phys. **232**, 37 (1998).
[11] F. Castet, L. Ducasse, and A. Fritsch, J. Chem. Phys. **112**, 10625 (2000).
[12] G. Brunaud, F. Castet, A. Fritsch, M. Kreissler, and L. Ducasse, J. Phys. Chem. B **105**, 12665 (2001).
[13] G. Brunaud, F. Castet, A. Fritsch, and L. Ducasse, Phys. Chem. Chem. Phys. **4**, 6072 (2002).
[14] G. Brunaud, F. Castet, A. Fritsch, and L. Ducasse, Phys. Chem. Chem. Phys. **5**, 2104 (2003).
[15] F. Castet, A. Fritsch, and L. Ducasse, Int. J. Quantum Chem. **106**, 734 (2006).
[16] M. J. S. Dewar, R. C. Bingham, and D. H. Lo, J. Am. Chem. Soc. **97**, 1285 (1975).
[17] M. J. S. Dewar and W. Thiel, J. Am. Chem. Soc. **99**, 4899 (1977).
[18] M. J. S. Dewar, E. G. Zoebisch, E. F. Healy, and J. J. P. Stewart, J. Am. Chem. Soc. **107**, 3902 (1985).
[19] J. J. P. Stewart, J. Comput. Chem. **10**, 209 (1989).
[20] J. Li and R. McWeeny, Int. J. Quantum Chem. **89**, 208 (2002).
[21] P. O. Löwdin, Phys. Rev. **97**, 1474 (1955).
[22] C. P. Brock and J. D. Dunitz, Acta Crystallogr., Sect. B: Struct. Sci. **46**, 795 (1990).
[23] See EPAPS document No. E-PRBMDO-77-090811 for the figures

provided in this document, which are labeled S1–S5 in the text. This document can be reached through a direct link in the online article's HTML reference section or via the EPAPS home page (http://www.aip.org/pubser's/epaps.html).

[24] The tensorial components of the quadrupole moment have been obtained indirectly by applying a scaling factor adjusted to reproduce the experimental data for benzene. See I. Eisenstein and R. W. Munn, Chem. Phys. **77**, 47 (1983).

[25] C. L. Cheng, D. S. N. Murthy, and G. L. D. Ritchie, Aust. J. Chem. **25**, 1301 (1972); R. J. W. LeFevre, L. Radom, and G. L. D. Ritchie, J. Chem Soc. B **775**, 507 (1968).

[26] S. Verlaak and P. Heremans, Phys. Rev. B **75**, 115127 (2007).

[27] E. A. Silinsh and V. Čápek, *Organic Molecular Crystals* (AIP, New York, 1994).

[28] E. V. Tsiper and Z. G. Soos, Phys. Rev. B **64**, 195124 (2001).

[29] E. Clementi, C. C. J. Roothan, and M. Yoshimine, Phys. Rev. **127**, 1618 (1962).

[30] A Troisi and G. Orlandi, J. Phys. Chem. A **110**, 4065 (2006).

[31] R. M. Glaeser and R. S. Berry, J. Chem. Phys. **44**, 3797 (1966).

[32] P. Petelenz, Chem. Phys. Lett. **103**, 369 (1984).

[33] M. N. Bussac, J. D. Picon, and L. Zuppiroli, Europhys. Lett. **66**, 392 (2004).

[34] J. L. Brédas, D. Beljonne, V. Coropceanu, and J. Cornil, Chem. Rev. (Washington, D.C.) **104**, 4971 (2004), and references therein.

[35] E. F. Valeev, V. Coropceanu, D. A. da Silva Filho, S. Salman, and J. L. Brédas, J. Am. Chem. Soc. **128**, 9882 (2006).

[36] K. Senthilkumar, F. C. Grozema, C. F. Guerra, F. M. Bickelhaupt, F. D. Lewis, Y. A. Berlin, M. A. Ratner, and L. D. A. Siebbeles, J. Am. Chem. Soc. **127**, 14894 (2005).

[37] K. Senthilkumar, F. C. Grozema, F. M. Bickelhaupt, and L. D. A. Siebbeles, J. Chem. Phys. **119**, 9809 (2003).

[38] A. A. Voityuk, J. Jortner, M. Bixon, and N. Rösch, J. Chem. Phys. **114**, 5614 (2001); N. Leulliot, M. Ghomi, G. Scalmani, and G. Berthier, J. Phys. Chem. **103**, 8716 (1999); I. Daizadeh, J. N. Gehlen, and A. A. Stuchebrukhov, J. Chem. Phys. **106**, 5658 (1997); D. J. Katz, and A. A. Stuchebrukhov, *ibid.* **109**, 4960 (1998).